

Optical Measurement of Photorecombination Time Delays

Graham G. Brown,* Chunmei Zhang,† Dong Hyuk Ko, and Paul B. Corkum
Joint Attosecond Science Laboratory, University of Ottawa & National Research Council of Canada
25 Templeton Street, Ottawa, Ontario, Canada K1N 5M6
(Dated: April 27, 2021)

Measuring the photoionization time delay between electrons from different orbitals is one of the most important accomplishments of attosecond science [1]. These measurements are typically done using attosecond pulses generated through electron recollision to photoionize a target inside a photoelectron spectrometer [2]. In such experiments, the measured delay corresponds to the superposition of all possible paths to ionization and can include multiple sources of delay [3–8]. These effects can be difficult to deconvolve [9]. Here, we exploit the collision physics nature of recollision and show that, by perturbing recollision dynamics [10], photorecombination time delays due to electron dynamics and structure can be measured entirely optically and without obfuscation from ionic structural and propagation effects [11]. This work paves the way for the entirely optical measurement of ultrafast electron dynamics and photorecombination delays due to electronic structure, multielectron interaction, and strong-field driven dynamics in complex molecular systems and correlated solid-state systems.

Cooper minima are ubiquitous in photoionization spectra from atoms and molecules [12]. The dipole transition matrix element coupling continuum states to a ground state wavefunction exhibiting a radial node passes through zero, leading to a spectral minimum and corresponding phase jump in photoionization spectra. The rapid phase variation across a Cooper minimum gives rise to significant photoionization time delays which have been measured using attosecond techniques [13]. As the inverse process of photoionization [14], photorecombination also exhibits Cooper minima, most notably in high-harmonic generation (HHG) [15, 16]. The spectral phase of attosecond pulses generated by recollision in such media are significantly shaped by photorecombination time delays around Cooper minima [6].

Photoionization time delays are typically measured using attosecond pulses to photoionize a target within a photoelectron spectrometer. These measurements require complicated experimental devices in addition to the equipment used for attosecond pulse generation. Further, there are several possible sources of delay which can include ionic or electronic structure, field-driven electron dynamics, and dispersive propagation effects [3–8]. Consequently, interpretation can be ambiguous.

Here, we report an approach to the study of ultrafast electron dynamics and photorecombination time delays using recollision which melds the precision of optics with collision physics. We show that attosecond in situ methods, which manipulate the electron-ion collision but observe the results optically, permit the measurement of photorecombination time delays attributable to strong-field driven electron dynamics and structure. We do this by studying the recombination phase around the Cooper

minimum in argon experimentally and confirm our interpretation using simulations based on time-dependent density functional theory (TD-DFT). We then use the semi-classical strong-field approximation (SFA) description of recollision to show that these methods are invariant to ionic structure.

The process of recollision leading to attosecond pulse emission consists of three steps [17]: (1) in the presence of a strong field, an electron tunnels into the continuum, (2) the electron is accelerated by the strong field, and (3) the electron recombines with its parent ion. In sinusoidal fields, these three-steps repeat every half optical-cycle. We generate an isolated attosecond pulse in argon using polarization gating [18], which involves superposing left- and right-circularly polarized pulses separated by a small-time delay. In regions where the pulses overlap with equal amplitude, the superposition of the counter-rotating fields results in linear polarization. Since recollision is extremely sensitive to the ellipticity of the driving field [19], attosecond pulse emission is confined to this overlap region, resulting in the emission of an isolated attosecond pulse.

Several variants of in situ measurement exist [10, 20]. For our experiment, we use a non-collinear method ideally suitable for characterizing isolated attosecond pulses [21]. The experimental diagram is shown in Figure 1 (a). We focus a 12 fs, polarization gated driving pulse of wavelength 1.8 μm into an argon gas jet, as shown by the red pulse. The pulse reaches an estimated peak intensity of $1 \times 10^{14} \text{ W cm}^{-2}$ within the jet.

We perturb recollision with a second-harmonic of the driving pulse with a relative intensity of 10^{-4} and at an angle of 6.9 mrad with respect to the driving field, delayed by a time τ , as depicted by the blue pulse. In the gas jet, the perturbing field modulates the recollision trajectories, resulting in a frequency-dependent modulation of the near-field attosecond pulse wavefronts. These modulations deflect the far-field attosecond pulse by an angle θ (in the figure, from purple to blue). As the delay

* graham.brown@uottawa.ca; These authors contributed equally to this work

† chunmei.zhang@uottawa.ca; These authors contributed equally to this work

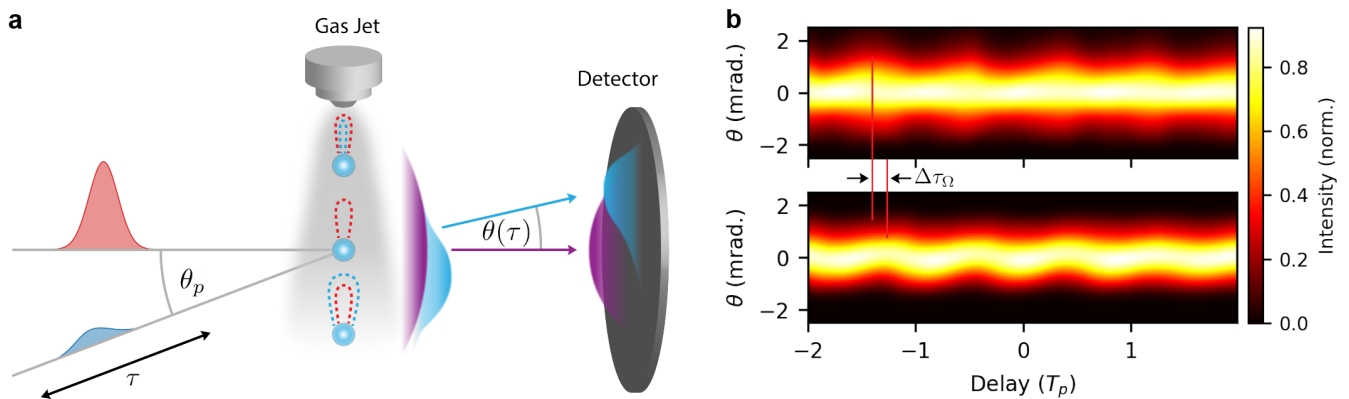


FIG. 1. (a) The polarization-gated driving pulse (red) and perturbing pulse delayed by time τ (blue) are focused into an argon gas jet. The perturbing pulse has a relative peak intensity of 10^{-4} and incident angle of $\theta_p = 30$ mrad with respect to the driving field. The perturbation induces a delay dependent modulation of the electron trajectories across the beam front from red to blue. The XUV wavefronts are modulated in the near field (from purple to blue), which results in a deflection of the XUV beam in the far-field by a delay-dependent angle $\theta(\tau)$. (b) The deflection of the XUV emission is recorded over a range of delays (in units of the perturbing field period T_p) and spectrally resolved. The resultant spectrograms for XUV energies of 60 (top) and 80 (bottom) are shown. The phase difference of the deflection modulations is proportional to the difference in emission time, $\Delta\tau(\Omega)$ between the two energies.

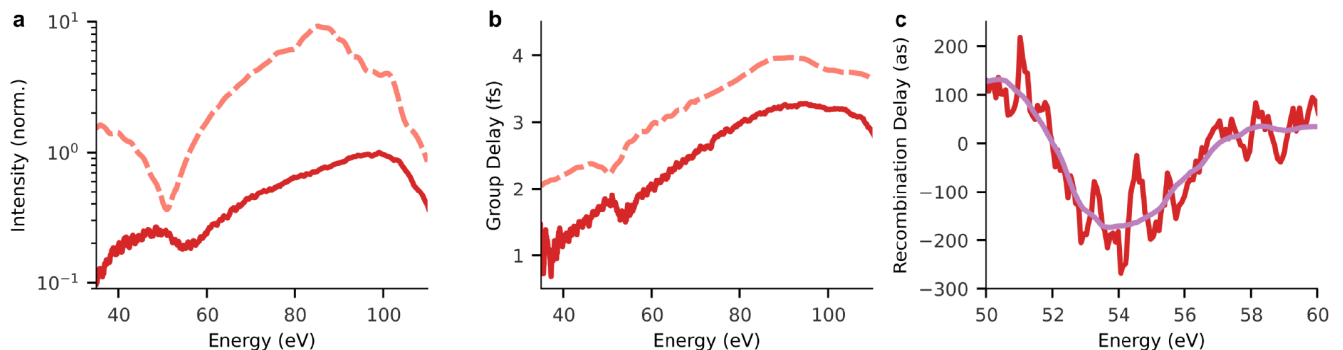


FIG. 2. (a) Measured intensity spectrum and (b) group delay for the attosecond pulse generated in argon (solid line) by a 12 fs $1.8 \mu\text{m}$ driving field with a peak intensity of $1 \times 10^{14} \text{ W cm}^{-2}$. The dashed lines show the spectrum and group delay from a TD-DFT simulation of the experimental conditions. (c) Difference between the measured group delay and the expected semi-classical result in the spectral region of the Cooper minimum before (red) and after (magenta) smoothing the data.

between the perturbing and strong fields is varied, the angular deflection of each spectral component of the XUV emission will modulate. The phase of this modulation is proportional to the XUV emission time. Figure 1 (b) shows the resultant spectrograms for XUV frequencies 60 (top) and 80 eV (bottom). The difference in the modulation phase is proportional to the difference in XUV emission times for these energies [21].

This process is performed for each spectral component of the measured attosecond pulse and we determine the group delay of the recollision electron using the relative delay of each spectral component with respect to that of a fixed energy. Please see methods where this is discussed. The unperturbed attosecond pulse spectrum is shown in Figure 2 (a) in red, where the Cooper minimum is observed near 55 eV. The attosecond pulse spectrum from

a TD-DFT simulation of the experimental conditions is shown by the dashed line (scaled $\times 10$ for clarity). The position of the Cooper minimum in the TD-DFT simulation, near 50 eV, is lower than the experimental result, but it is well-known that the position of the Cooper minimum in HHG is sensitive to phase-matching conditions [22].

The measured group delay is shown in Figure 2 (b), where the experimental data is shown as a solid red line and the simulated result is shown by a dashed line. Both the experimental and theoretical group delay curves are predominantly linear up until the cut-off energy near 90 eV. Both, however, exhibit a variation in the group delay near the Cooper minimum. Therefore, the experimental and theoretical results agree.

The difference between the experimentally measured

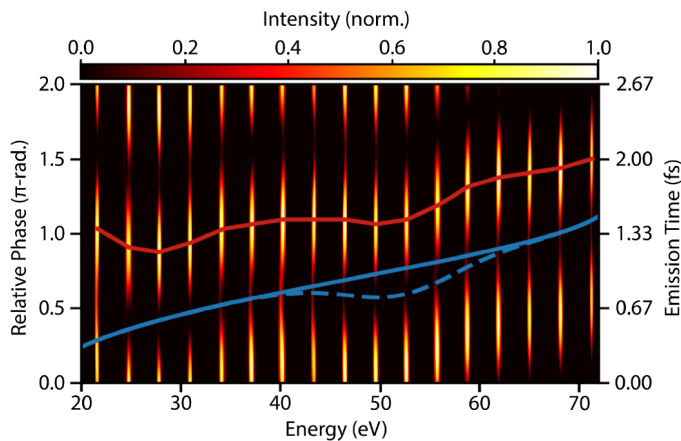


FIG. 3. The normalized even-harmonic spectrogram from the TD-DFT simulation of an $\omega - 2\omega$ in situ measurement in argon. The overlaid red line shows the relative phase which maximizes each even harmonic signal from the simulation. The overlaid solid (dashed) shows the expected result for the maximizing relative phase from the semi-classical model without (with) the recombination phase around the Cooper minimum. The blue lines are shifted by $\pi/2$ for clarity.

result and the expected semi-classical group delay in the absence of recombination effects is the photorecombination time delay. This is shown in Figure 2 (b) in red with a smoothed curve in magenta. The maximum delay difference around the Cooper minimum near 54 eV is 160 as. The measured result agrees with studies of photorecombination time delays in argon [6].

We confirm our interpretation by simulating an in situ measurement using TD-DFT [23] and a collinear second-harmonic perturbing field instead of the non-collinear geometry in the experiment. While co-linear fields are usually used to characterize attosecond pulse trains [10], here we use them to demonstrate the sensitivity of in situ measurement to the recombination phase while simultaneously taking advantage of the simpler collinear geometry for simulations.

With co-linear fields, the perturbation breaks the half-cycle asymmetry of recollision, resulting in the emission of even harmonics. The perturbation imparts a controlled phase difference between trajectories that are separated by half a laser period, thereby controlling the phase of photon emission at a given energy in adjacent half-cycles. This phase difference depends on the relative phase between the perturbing and driving fields. As the relative phase is scanned, the intensity of each even harmonic modulates periodically with a phase offset proportional to its emission time and, therefore, the relative phase which maximizes (or minimizes) the even-harmonic signal is also proportional to the emission time. This is expounded in the methods section. The qualitative differences between the experimental and theoretical measurement methods do not detract from the point of this letter.

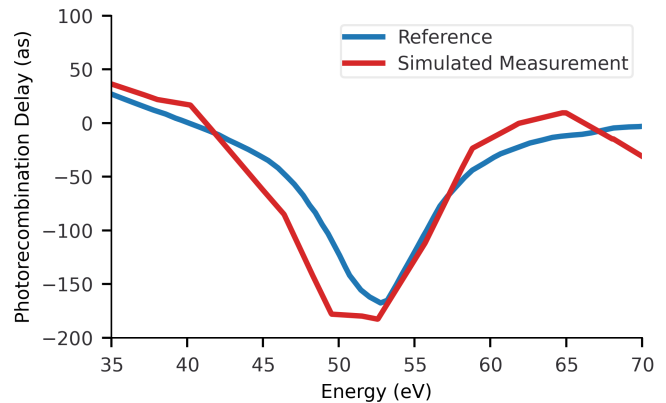


FIG. 4. A comparison of the photorecombination time delay reconstructed from the simulated spectrogram in Figure 3 and calculated photorecombination time delay time delay from argon around the Cooper minimum [6].

We simulate high-harmonic generation in argon using an 800 nm driving pulse with a peak intensity of $2.75 \times 10^{14} \text{ W cm}^{-2}$ and pulse duration of 20 fs, corresponding to a semi-classical cut-off near 70 eV. As in the experiment, we use a second harmonic intensity that is 10^{-4} of the fundamental.

The spectrogram from the simulated in situ measurement is shown in Figure 3. The contour plot shows the normalized even harmonic spectrum plotted with respect to the relative phase between the driving and perturbing pulses on the left axis. The overlaid red line shows the maximizing relative phase for each even harmonic and the right axis shows the emission time calculated from the maximizing phase. The result deviates from the expected linear chirp near the ionization threshold (i.e. below 25 eV) and around the Cooper minimum, where a prominent decrease in emission time is observed.

The overlaid solid blue line shows the expected maximizing phase for recollision from an argon atom with a flat recombination phase calculated using the SFA [24] (shifted by $\pi/2$ for clarity). The linearity indicates that the variation observed in the TD-DFT result around the Cooper minimum can be attributed to recombination effects. We verify this by including a Lorentzian π -phase jump around 52 eV with a bandwidth of 10 eV in the transition moment and SFA analysis (see supplementary section). The maximizing phase calculated from the SFA when including this transition moment phase is shown by the dashed blue line and agrees with both the simulated and experimental in situ measurements.

The photorecombination delay is determined by finding the emission times for each even harmonic from the maximizing phase in Figure 3 and subtracting the expected semi-classical emission time. This is depicted in Figure 4 in red and compared with a reference photorecombination delay in blue [6]. The photorecombination time delay from the simulated measurement exhibits a

delay of nearly -175 as, in agreement with the experimental results in Figure 2. The differences between the simulated measurement and the reference photorecombination delay can be attributed to the energy resolution of the measurement technique and the dynamics near the high-harmonic cut-off of 70 eV. This validates our interpretation of the experimental measurement and demonstrates the feasibility of in situ techniques to measure photorecombination time delays.

Photorecombination time delays can also arise due to ionic structure [25], but these time delays cannot be measured using attosecond in situ techniques [11]. This is the critical difference between photoionization-based and in situ measurement. To understand why, it is useful to turn to the SFA. If we consider a simple atom, a recollision trajectory can be characterized by three parameters: the stationary momentum k , the time of ionization t_b , and the time of recombination and photon emission t_r . If we perturbatively include a momentum-dependent transition moment phase, $\Phi_{re}(k)$, the first-order correction to the emission time, $\Delta t_r^{(1)}$ is given as follows (atomic units are used):

$$\Delta t_r^{(1)} = \frac{1}{k + A(t_r)} \left. \frac{\partial \Phi_{tr}}{\partial k} \right|_{k+A(t_r)}, \quad (1)$$

where $A(t)$ is the vector potential of the driving field.

When considering a molecular system, trajectories ionizing from and recombining to each atomic centre must be considered [26]. When compared with a simple atom, the changes to individual trajectory emission times is the time required for an electron to travel the distance from the origin to the recombination atomic centre. Only when all trajectories are superposed does the emitted attosecond pulse exhibit a phase jump. Attosecond in situ methods characterize these trajectories individually, but not the emitted pulse, and the effects of the internuclear separation cancel (see supplementary section). Thus, in situ methods are invariant with respect to ionic structure.

The Cooper minimum is a result of the shape of the ground state wavefunction itself and is contained within a single path to recombination. Consequently, the correction to the recombination time reflects the shape of the phase jump and affects the trajectories which lead to attosecond pulse emission. This is shown in Figure 5, which shows the electron trajectories calculated using the SFA leading to photon emission at 30 (blue), 50 (red), and 70 eV (purple) from an argon atom with (solid) and without (dashed) a Lorentzian π -phase jump at 50 eV in its transition moment. Away from the minimum, the trajectories leading to the emission of photon energies 30 and 70 eV from both systems are nearly equal with negligible differences in the times of recombination.

The trajectories leading to photon emission at 50 eV from the argon atom with and without the transition moment phase jump are quite different, with both the times of birth and recombination differing considerably. As implied by the saddle-point analysis used in the SFA,

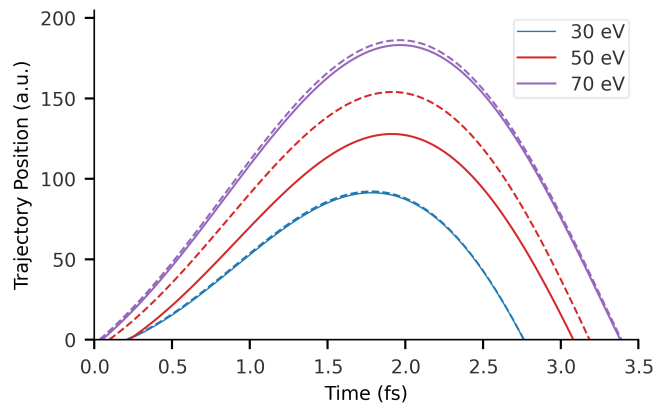


FIG. 5. Semi-classical electron trajectories from an argon atom with (solid) and without (dashed) a π -phase jump around the Cooper minimum at 50 eV for photon energies 30 (blue), 50 (red), and 70 eV (purple). For the off-resonance energies of 30 and 70 eV, the trajectories from both atomic systems are similar and exhibit negligible differences in recombination time. For the trajectories leading to emission at 50 eV, the trajectories from the atom with and without the recombination phase are significantly different due to the recombination phase variation.

trajectories only with an appropriate phase will sum constructively and result in XUV emission. When a varying recombination phase is present, this phase will in part determine which trajectories dominate attosecond pulse emission and, therefore, in situ measurement will detect its effect. This agrees with studies which show continuum and recombination dynamics are interrelated [7, 27] and calls into question the application of methods describing recollision which decouple propagation dynamics from recombination effects [14].

In conclusion, both experimentally and theoretically, we have demonstrated an entirely optical measurement of photorecombination time delays by modulating recollision dynamics in argon. Ours is a hybrid approach, in keeping with recollision, in which we exploit the optical coherence of high harmonic generation and the conceptual simplicity of a collision experiment. While photoionization and photorecombination are directly related in many ways, photoionization time delay measurements require a sophisticated photoelectron spectrometer in addition to the attosecond pulse generation apparatus, hindering the widespread study of photoionization time delays. Furthermore, photoionization measurements are encumbered by the sensitivity to many possible sources of delay including electron dynamics, ionic structure, and dispersive effects during attosecond pulse propagation, leading to a lack of clarity of the meaning of the measurement.

In addition, our all-optical approach can be readily generalized to studying collision induced plasmon excitation, Fano resonances and other multielectron effects, extending to gas-phase molecules and possibly to solids.

This will include processes such as recollision-induced plasmon excitation and other multielectron processes. Since photoionization and photorecombination experiments measure different things, combining them will allow us to unambiguous isolation of time delays associated with ionic structural and electron dynamics effects. Any laboratory capable of generating high harmonics can perform these studies.

Finally, photorecombination time delay measurements, open a new approach to attosecond pulse shaping in which the spectral phase structure of a passive external filter is replaced by the spectral phase structure of the transmission moment that can be controlled using external fields.

I. ACKNOWLEDGEMENTS

This research was supported by the United States Air Force Office of Scientific Research (award #: FA9550-16-1-0109) with contributions from the Canada Foundation for Innovation, the Canada Research Chairs program, Canada's Natural Sciences and Engineering Research Council and the National Research Council of Canada.

Appendix A: Methods

1. Experimental System

The 1.8 μm driving laser pulses in this experiment are delivered by a commercial optical parametric amplifier (HE-TOPAS, Light Conversion) which is pumped with a chirped-pulse-amplified Ti:Sapphire laser system (Thales, Alpha 100). The OPA system provides 50 fs laser pulses at 1.8 μm at a repetition rate of 100 Hz. The pulses are further amplified by a home built OPA booster stage to get more than 1 mJ pulse energy and then focused into an argon-filled, differentially pumped hollow-core fibre (1 m long, 400 μm inside diameter) by an $f = 75$ cm CaF_2 lens. The spectrum is broadened with 0.8 bar argon gas in the hollow-core fibre and the residual chirp is compensated with an antireflection coated fused silica plate in the beam path. The spectrum after the propagation through the fibre is shown in Figure S1 (a). A pair of fused silica wedges is used for dispersion fine tuning and CEP absolute value controlling. We achieve 650 μJ sub-12 fs pulses from the fibre compressor, as shown in Figure S1 (b). The CEP of the 1.8 μm laser pulses was measured with a homebuilt $f - 2f$ interferometer and locked by a servo system.

The laser beam after the fiber compressor is divided by a dichroic beam splitter after the second harmonic generation with a 200 μm -thick BBO crystal. The transmitted fundamental beam passed through a quartz plate with thickness of 300 μm and a broadband quarter-wave plate

to create a polarization gated beam for single attosecond pulse generation. The reflected second harmonic, as a perturbation, after passing through a half waveplate, combined with fundamental beam parallelly by a D shape mirror and the perturbation beam is 2 mm below the fundamental.

Both beams are focused into the chamber by a silver-coated concave mirror ($f = 30$ cm) into the gas jet. The angle of between two beams is ~ 6.7 mrad and their intensity ratio was $\sim 10^{-4}$. The time delay between two beams is controlled by a closed loop piezo stage (Thorlabs) with delay step of 66.4 as. In the chamber, the gas source is from a pulsed argon gas jet with a backing pressure of 4.5 bars. The location of the gas jet is ~ 4 mm before the fundamental focus to enhance the short trajectory and a continuous spectrum extending from 30 eV to 110 eV is obtained. The peak intensity at the focus is $\sim 5 \times 10^{14}$ W cm^{-2} and the intensity at the jet position is estimated to be 1×10^{14} W cm^{-2} by the high harmonic cut-off. The high harmonics propagate through a slit, frequency-resolved by a curved 1200 l/mm grating (Shimadzu, 30-002) and are recorded on a microchannel plate (Photonis, Chevron) with a CCD detector.

2. Experimental Temporal Characterization

The phase modulation induced by the perturbing field can be expressed as follows:

$$\sigma_{\Omega}(y, \tau) = A_{\Omega} \sin(k_p \theta_p (y - c\tau/\theta_p) + \Phi_{\Omega}), \quad (\text{A1})$$

where k_p is the perturbing pulse wavenumber of the perturbing field, θ_p is the relative angle between the perturbing and driving fields, y is the vertical position in the gas jet, c is the speed of light, τ is the delay between the perturbing and driving fields, and, for photon emission at frequency Ω , the terms A_{Ω} and Φ_{Ω} represent the frequency-dependent amplitude and phase of the modulation. The phase of the modulation depends linearly on the XUV emission time [10]. The difference in phase between two different frequencies can be directly observed from the XUV spectrum, as shown in Figure 1 (b), where this difference is mapped to a difference in emission, $\Delta\tau_{\Omega}$. The relative emission time of the entire spectrum is determined by determining the change in phase Φ_{Ω} from each spectral component's modulation relative to that of a fixed energy.

3. Simulated In Situ Measurement

For the simulated collinear in situ measurement, we consider HHG in Ar driven and perturbed by sinusoidal vector potential fields $A(t)$ and $A_p(t, \phi)$, respectively:

$$A(t) = A_0 \sin(\omega_0 t), \quad (\text{A2})$$

$$A_p(t, \phi) = \eta A_0 \sin(2\omega_0 t + \phi), \quad (\text{A3})$$

where A_0 is the driving field amplitude, ω_0 is the fundamental field frequency, η is the relative amplitude of the perturbing and driving fields, and ϕ is the relative phase between the driving and perturbing fields. The phase modulation due to the perturbing field is given as follows [10]:

$$\sigma_\Omega(t_r, \phi) = \sigma(t_r) \cos(\phi - \theta(t_r)), \quad (\text{A4})$$

where k_Ω is the electron momentum and t_r is the time of recombination. For perfectly sinusoidal fields,

$$\theta(t_r) = \omega_0(t_r + t_b), \quad (\text{A5})$$

where t_b is the time of ionization. With this, the dipole moment leading to emission of harmonic $2N$ at time t_{2N} for integer N satisfies the following:

$$\tilde{D}(2N\omega_0) \propto \cos(\phi - \theta(t_{2N})). \quad (\text{A6})$$

The even-harmonic intensity modulates according to

$$\left| \tilde{D}(2N\omega_0) \right|^2 \propto \cos^2(\phi - \theta(t_{2N})), \quad (\text{A7})$$

which is maximized when

$$\phi = \theta(t_{2N}). \quad (\text{A8})$$

Thus, tracking the phases which is maximize or minimize the even-harmonic signal provides a measurement of the harmonic emission time.

-
- [1] E. Goulielmakis, Z.-H. Loh, A. Wirth, R. Santra, N. Rohringer, V. S. Yakovlev, S. Zherebtsov, T. Pfeifer, A. M. Azzeer, M. F. Kling, S. R. Leone, and F. Krausz, Real-time observation of valence electron motion, *Nature* **466**, 739 (2010).
- [2] L. Cattaneo, J. Vos, M. Lucchini, L. Gallmann, C. Cirelli, and U. Keller, Comparison of attosecond streaking and rbbitt, *Opt. Express* **24**, 29060 (2016).
- [3] T.-Y. Du, D. Tang, X.-H. Huang, and X.-B. Bian, Multichannel high-order harmonic generation from solids, *Phys. Rev. A* **97**, 043413 (2018).
- [4] K. V. J., Y. Mairesse, B. Carré, M. B. Gaarde, P. Johnsson, S. Kazamias, R. López-Martens, J. Mauritsson, K. J. Schafer, P. Balcou, A. L’huillier, and P. Salières, Frequency chirp of harmonic and attosecond pulses, *Journal of Modern Optics* **52**, 379 (2005), <https://doi.org/10.1080/09500340412331301542>.
- [5] C. Vozzi, F. Calegari, E. Benedetti, R. Berlasso, G. Sansone, S. Stagira, M. Nisoli, C. Altucci, R. Velotta, R. Torres, E. Heesel, N. Kajumba, and J. P. Marangos, Probing two-centre interference in molecular high harmonic generation, *Journal of Physics B: Atomic, Molecular and Optical Physics* **39**, S457 (2006).
- [6] S. B. Schoun, R. Chirla, J. Wheeler, C. Roedig, P. Agostini, L. F. DiMauro, K. J. Schafer, and M. B. Gaarde, Attosecond pulse shaping around a cooper minimum, *Phys. Rev. Lett.* **112**, 153001 (2014).
- [7] S. Pabst and R. Santra, Strong-field many-body physics and the giant enhancement in the high-harmonic spectrum of xenon, *Phys. Rev. Lett.* **111**, 233005 (2013).
- [8] C. Goldsmith, A. Jaroń-Becker, and A. Becker, Attosecond streaking time delays: Finite-range interpretation and applications, *Applied Sciences* **9**, 492 (2019).
- [9] S. Nagele, R. Pazourek, M. Wais, G. Wachter, and J. Burgdörfer, Time-resolved photoemission using attosecond streaking, *Journal of Physics: Conference Series* **488**, 012004 (2014).
- [10] N. Dudovich, O. Smirnova, J. Levesque, Y. Mairesse, M. Y. Ivanov, D. M. Villeneuve, and P. B. Corkum, Measuring and controlling the birth of attosecond xuv pulses, *Nature Physics* **2**, 781 (2006).
- [11] M. Spanner, J. B. Bertrand, and D. M. Villeneuve, In situ attosecond pulse characterization techniques to measure the electromagnetic phase, *Phys. Rev. A* **94**, 023825 (2016).
- [12] J. W. Cooper, Photoionization from outer atomic subshells. a model study, *Phys. Rev.* **128**, 681 (1962).
- [13] R. Pazourek, S. Nagele, and J. Burgdörfer, Time-resolved photoemission on the attosecond scale: opportunities and challenges, *Faraday Discuss.* **163**, 353 (2013).
- [14] A.-T. Le, R. R. Lucchese, S. Tonzani, T. Morishita, and C. D. Lin, Quantitative rescattering theory for high-order harmonic generation from molecules, *Phys. Rev. A* **80**, 013401 (2009).
- [15] J. Higuete, H. Ruf, N. Thiré, R. Cireasa, E. Constant, E. Cormier, D. Descamps, E. Mével, S. Petit, B. Pons, Y. Mairesse, and B. Fabre, High-order harmonic spectroscopy of the cooper minimum in argon: Experimental and theoretical study, *Phys. Rev. A* **83**, 053401 (2011).
- [16] M. C. H. Wong, A.-T. Le, A. F. Alharbi, A. E. Boguslavskiy, R. R. Lucchese, J.-P. Brichta, C. D. Lin, and V. R. Bhardwaj, High harmonic spectroscopy of the cooper minimum in molecules, *Phys. Rev. Lett.* **110**, 033006 (2013).
- [17] P. B. Corkum, Plasma perspective on strong field multiphoton ionization, *Phys. Rev. Lett.* **71**, 1994 (1993).
- [18] D. Oron, Y. Silberberg, N. Dudovich, and D. M. Villeneuve, Efficient polarization gating of high-order

- harmonic generation by polarization-shaped ultrashort pulses, *Phys. Rev. A* **72**, 063816 (2005).
- [19] A. Flettner, J. König, M. B. Mason, T. Pfeifer, U. Weichmann, G. Gerber, and R. Duren, Ellipticity dependence of atomic and molecular high harmonic generation, *European Physical Journal D, Atomic, Molecular and Optical Physics* **21**, 115 (2002), cONDENSED MATTER PHYSICS, SUPERCONDUCTIVITY AND SUPERFLUIDITY.
- [20] K. T. Kim, D. M. Villeneuve, and P. B. Corkum, Manipulating quantum paths for novel attosecond measurement methods, *Nature Photonics* **8**, 187 (2014).
- [21] K. T. Kim, C. Zhang, A. D. Shiner, S. E. Kirkwood, E. Frumker, G. Gariépy, A. Naumov, D. M. Villeneuve, and P. B. Corkum, Manipulation of quantum paths for space-time characterization of attosecond pulses, *Nature Physics* **9**, 159 (2013).
- [22] J. P. Farrell, L. S. Spector, B. K. McFarland, P. H. Bucksbaum, M. Gühr, M. B. Gaarde, and K. J. Schafer, Influence of phase matching on the cooper minimum in ar high-order harmonic spectra, *Phys. Rev. A* **83**, 023420 (2011).
- [23] N. T. Maitra, Perspective: Fundamental aspects of time-dependent density functional theory, *The Journal of Chemical Physics* **144**, 220901 (2016), <https://doi.org/10.1063/1.4953039>.
- [24] M. Lewenstein, P. Balcou, M. Y. Ivanov, A. L’Huillier, and P. B. Corkum, Theory of high-harmonic generation by low-frequency laser fields, *Phys. Rev. A* **49**, 2117 (1994).
- [25] F. Mauger, P. M. Abanador, T. D. Scarborough, T. T. Gorman, P. Agostini, L. F. DiMauro, K. Lopata, K. J. Schafer, and M. B. Gaarde, High-harmonic spectroscopy of transient two-center interference calculated with time-dependent density-functional theory, *Structural Dynamics* **6**, 044101 (2019).
- [26] M. Labeye, F. m. c. Risoud, C. Lévêque, J. Caillat, A. Maquet, T. Shaaran, P. Salières, and R. Taïeb, Dynamical distortions of structural signatures in molecular high-order harmonic spectroscopy, *Phys. Rev. A* **99**, 013412 (2019).
- [27] D. Faccialà, S. Pabst, B. D. Bruner, A. G. Ciriolo, M. Devetta, M. Negro, P. P. Geetha, A. Pusala, H. Soifer, N. Dudovich, S. Stagira, and C. Vozzi, High-order harmonic generation spectroscopy by recolliding electron caustics, *Journal of Physics B: Atomic, Molecular and Optical Physics* **51**, 134002 (2018).